International Journal of Nanoelectronics and Materials

In Press, Accepted Manuscript – Note to user

Aluminum Doping for Enhancing Charge Photoanode ZnO Nanorod for DSSC

Iwanono Iwantono[1], Puji Nurahmawati[1], Sella Natalia[1], Romi Fadli Syahputra[1], Awitdrus Awitdrus[1], Zulkarnain Zulkarnain[1], Akrajas Ali Umar[2]

[1]Department of Physics Universitas Riau, Pekanbaru, Indonesia
[2]Institute of Microengineering and Nanoelectronics, Universiti Kebangsaan Malaysia, 43600, Selangor, Malaysia

ABSTRACT

Renewable energy sources are being developed as alternatives to fossil energy by several sources, such as solar cenergy and wind power. The progress on solar power conversion to electricity via solar cell is impressively developed to obtain the best performance and low cost production. We studied the dye-sensitized solar cell (DSSC) as it is cost-effective and environment friendly compared to the widely used silicon-based cells. However, the low current density and power conversion efficiency are the primary limitations of DSSCs, especially zinc oxide (ZnO)-based DSSCs. In this study, we enhanced the ZnO nanorod properties through aluminum (Al) doping. To find the optimum doping concentration, the concentration of Al was varied at 0%, 0.5%, 1.0%, 1.5%, and 2.0%. Al-doped ZnO nanorods were grown by a seed-mediated hydrothermal method at 90°C for 8 h. The morphological, structural, optical, and photovoltaic properties of these nanorods were analyzed by field emission scanning electron microscopy, X-ray diffraction, UV-Vis spectroscopy, and J-V curve analysis. ZnO nanorods with 1.0% Al doping demonstrated photovoltaic performance improvement up to 241.8%.

Keywords: Aluminum Doping, DSSC, Solar Cells, Renewable Energy, ZnO Nanorod

1. INTRODUCTION

Silicon-based solar cells were the first solar cells to have been commercialized successfully. The demand for silicon-based solar cells is increasing. Although the efficiency of these cells is high, they are expensive due to the use of complex production technology and lack of energy-efficient alternatives. Studies are ongoing to develop other types of solar cells. Dye-sensitized solar cell (DSSC) has been recently developed from photoelectrochemical solar cells with a demonstrated efficiency of 11%–13% [1,2]. A DSSC has a sandwich-like arrangement comprising active material, dye, electrolyte, and counter electrodes [1]. However, the primary limitations of DSSCs are that they have low current density and power conversion efficiency, especially zinc oxide (ZnO)-based DSSCs. ZnO, demonstrating a bandgap of 3.37 eV [3,4], is an active material with prospective applications.

ZnO nanomaterials have been widely used in DSSCs, which have an efficiency of ±0.3% [5]. Studies have been conducted to increase the efficiency value of DSSCs by doping, which can achieve transparency, stability, conductivity, and high electron mobility [6]. ZnO can be doped with group IIIA metals, including In, Al, Ga, and B [7]. Aluminum was chosen as a doping material because it is inexpensive, abundantly available, non-toxic, and non-corrosive, as well as demonstrates good conductance of heat and electricity [8]. ZnO nanomaterials can be doped using organic compounds containing aluminum metal, which increases the cell's electrical conductivity [9]. Alumunium dopant can enhace physical properties of ZnO nanomaterial fabrication through several variables [6]. Some physical parameters that affect the synthesis of Al-doped ZnO nanomaterials are concentration of the growing solution, time of growth, temperature of growth, temperature of annealing, and concentration of the dopant. In this study, we considered the dopant concentration [5].

*Corresponding author: iwantono@lectuere.unri.ac.id

The main objective of this work was to discover the optimum concentration of Al to be doped on ZnO nanorods that demonstrate high photovoltaic performances. Seed-mediated hydrothermal method was used to grow ZnO nanorods [5]. The dopant effects were investigated through morphological, structural, and optical analysis. Morphological and structural analyses reveal the structural shape and lattice parameter of the nanorods [10,11]. UV-Vis spectroscopy provides their spectral absorption and bandgap energy estimation. The performance test was conducted using artificial sunlight illumination (AM 1.5 G, which was provided by Gamry Framework EPHE 200 system)

2. MATERIALS AND METHODS

2.1 Seeding Preparation

Zinc acetate dihydrate (ZAD) seeding solution of 0.01 M was prepared by dissolving 0.022 g of ZAD in 10 mL ethanol. The seeding process was initiated by dripping the seeding solution on fluorine tin oxide (FTO) substrate in a spin coater at 3000 rpm for 30 s. Then, the sample was heated at 100˚C for 15 min. This process was repeated several times to obtain a uniform distribution of the ZnO seed of about 15 nm. The final step of the sample was carried out at 350˚C for 1 h [12].

2.2 Growing ZnO Nanorod

ZnO nanorod growth solution was prepared by mixing 0.5694 g of zinc nitrate hexahydrate (ZNH) solution, 0.2803 g of hexamethylenetetramine (HMT), and 0.1875 g of aluminum nitrate nonahydrate in 0.1 M deionized (DI) water. Next, the doping concentration was varied at 0%, 0.5%, 1.0%, 1.5%, 2.0%, and 2.5% over the concentration of the growing solution. Each sample was grown at 90°C for 8 h. The sample was then removed and cleaned using DI water and dried using a drier.

2.3 Characterization and Performance Test

The characteristics of the obtained ZnO nanorod were examined using field emission scanning electron microscopy (FESEM; Zeiss, Compact Co. Ltd.), X-ray diffraction (XRD; Bruker, EIXS), and UV-Vis spectroscopy (U-3900H). DSSCs were fabricated by assembling the sandwich-form [5], which consists of active material (Al-doped ZnO nanorods), dye N719, electrolytes (iodolyte AN-50), and counter electrodes (plat) with an active area 0.23 cm^2. The cell performance was tested under artificial sunlight illumination (AM 1.5 G, Gamry Framework EPHE 200; input power, 100 $mW.cm^{-2}$).

3. RESULTS AND DISCUSSION

3.1 Morphological Analysis

The FESEM images of the ZnO nanorod are presented in Figure 1 and the thickness of the rod is detailed in Figure 2. It was clear from the analysis that a wurtzite hexagonal structure of ZnO was obtained [13]. The various cross-sectional sizes that were obtained are presented in Table 1. Interestingly, 1.0% Al-doped ZnO nanorods demonstrate the smallest size and highest

thickness. Generally, Al-doping significantly increases the ZnO nanorod thickness and its density, as are presented in Figures 1 and 2 [7]. These results are in line with the research conducted by Zhou et al. [14] and Alkahlout et al. [15].

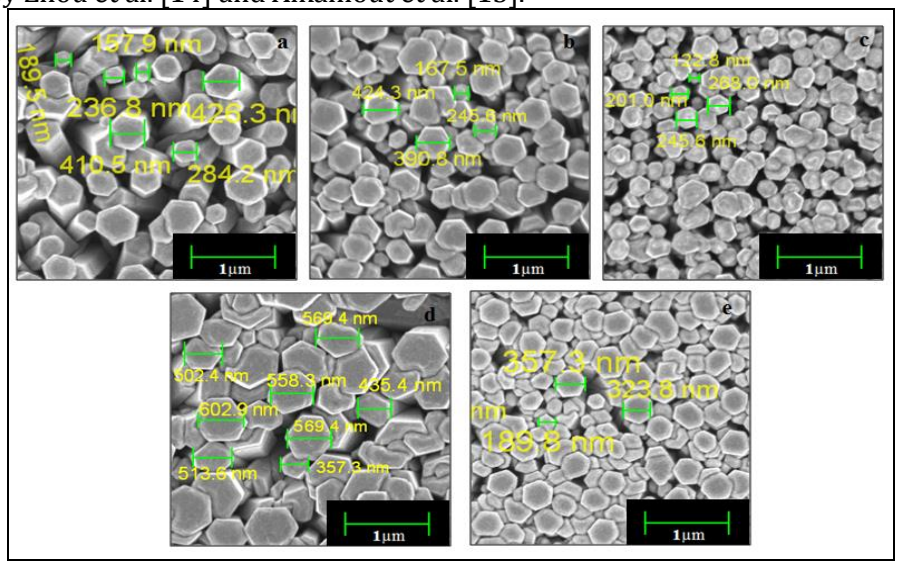

Figure 1. Field emission scanning electron microscopic images of the ZnO nanorod with (a) 0%, (b) 0.5%, (c) 1%, (d) 1.5%, and (e) 2% Al-doping. (Magnification, 10,000).

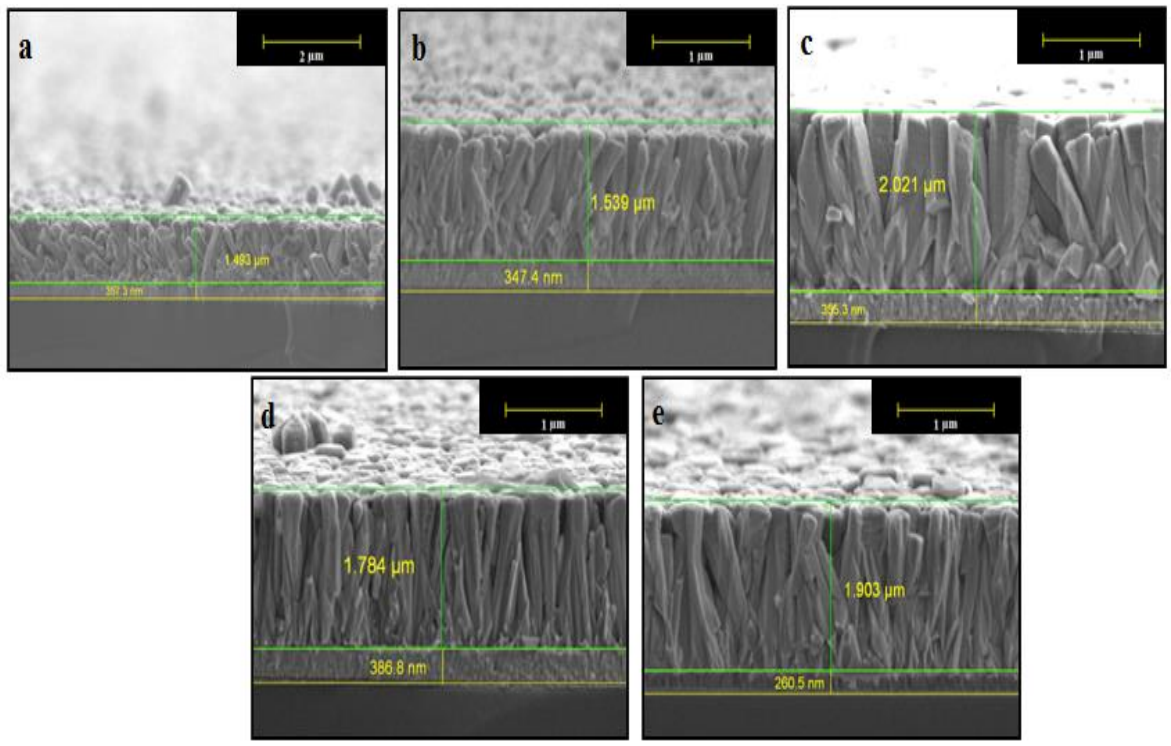

Figure 2. Thickness of each sample. (a) 0% (magnification, 20,000; bar scale, 2 µm), (b) 0.5%, (c) 1%, (d) 1.5%, and (e) 2%. (Magnification, 10,000; bar scale, 1 µm).

Table 1 Size and thickness of Al-doped ZnO nanorods

Al concentration (%)	Size (nm)	Thickness (μm)
0.0	157.9-426.3	1.493
0.5	167.5-424.3	1.539
1.0	122.8-268.0	2.021
1.5	223.3-609.2	1.784
2.0	189.3-357.3	1.903

3.2 Lattice Characteristics

The XRD pattern of Al-doped ZnO nanorods is presented in Figure 3. In the figure, the diffraction peaks appear at an angle of 2θ = 31.71°, 34.51°, 36.28°, 47.61°, and 56.54°, which correspond to a crystal plane of (100), (002), (101), (012), and (110). As can be seen in the figure, the highest XRD peak for all samples occurs at an angle of 2θ: 34.51°, with a crystal plane of (002). These results are consistent with those reported by Zhou et al. [14], Lee et al. [16], and Soaram et al. [7]. Concerning the percentage of Al concentration, the intensity increased at 0%, 0.5%, and 1.0% and decreased at 1.5% and 2.0%. The higher intensity in the XRD pattern corresponds to the denser nanostructure form [7]. In our study, 1.0% Al-doped ZnO nanorod growth was optimal.

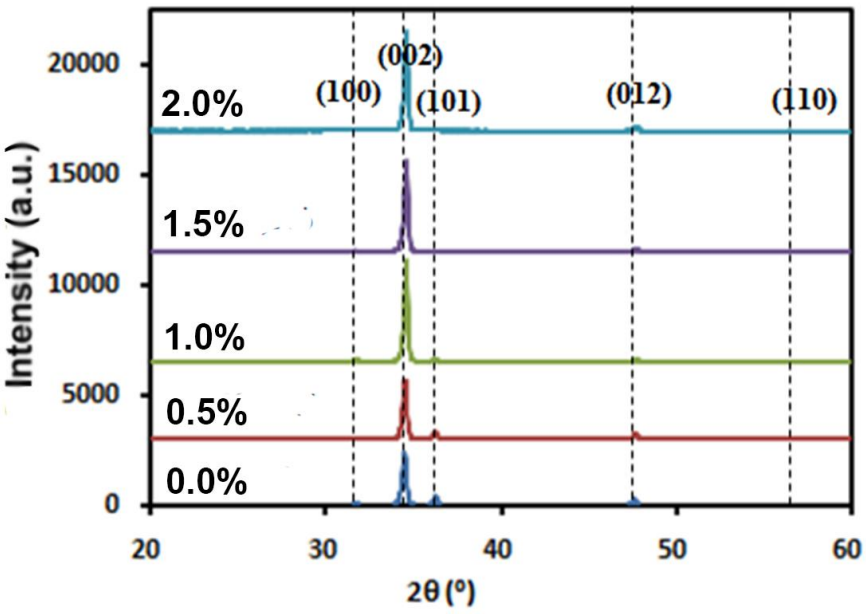

Figure 3. X-ray diffraction spectra of ZnO nanorods.

As can be seen in Figure 4, the angles of 2θ of field crystal orientation of ZnO nanorods (002) with Al concentrations of 0%, 0.5%, 1.0%, 1.5%, and 2.0% are 34.51°, 34.53°, 34.6°, 34.61°, and 34.61°, respectively. From the XRD pattern, we can see a shift of the 2θ angle in the field orientation (002) is 0.02°–0.10° dominant to the right (greater angle), which is in accordance with the findings of Soaram et al. [7] and Alkahlout et al. [15].

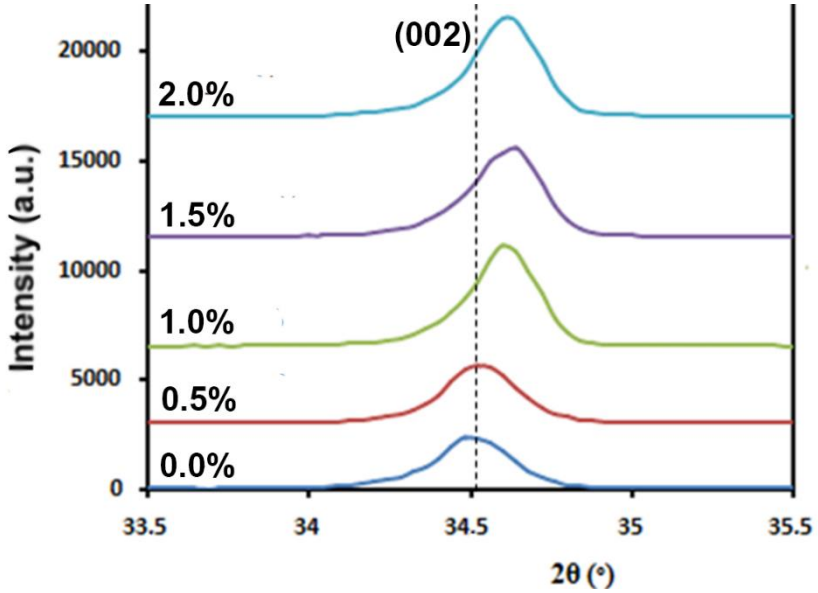

Figure 4. Peak-shift of X-ray diffraction spectra of (002) crystal orientation.

Table 2 Full width at half maximum (FWHM) and crystalline size of Al-doped ZnO nanorods.

Al concentration (%)	FWHM (°)	Crystalline size (nm)
0.0%	0.2538	32.793
0.5%	0.2431	34.242
1.0%	0.2175	38.276
1.5%	0.2319	35.899
2.0%	0.2200	37.456

The size of the Al-doped ZnO crystal can be determined using Scherrer's equation. The large Full Width at Half Maximum (FWHM) is inversely proportional to the crystal size; that is the smaller the FWHM, the higher is the crystallinity, because the atoms are arranged periodically and more regularly [17]. This happens because the large crystalline size supports a constructive interference. In Table 2, the crystal sizes of ZnO nanorods with Al concentrations of 0%, 0.5%, 1.0%, 1.5%, and 2.0% are, respectively, 32.793, 34.242, 38.276, 35.899, and 37.456 nm. Crystal size increased by 1%, but again decreased after administration of large Al doping of 1.0%. From

Figure 3, Figure 4, and Table 2, it can be concluded that the effect of varying the Aluminum doping concentration on the ZnO nanorod structure can arrange and control the lattice [7].

3.3 UV-Vis Absorption

The UV-Vis absorption spectrum of the sample is presented in Figure 5. The figure shows that strong absorption occurs at 320–385 nm, which is the common behavior of the ZnO nanorod [18]. In the figure, the absorption rates of all samples are nearly similar. The highest maximum absorption intensity was obtained by 3.670 a.u, a 1.0% Al-doped ZnO nanorod, which indicates that it has a higher density, in accordance with the FESEM and XRD analyses. The highest absorption spectra occurred at 350 nm for all samples.

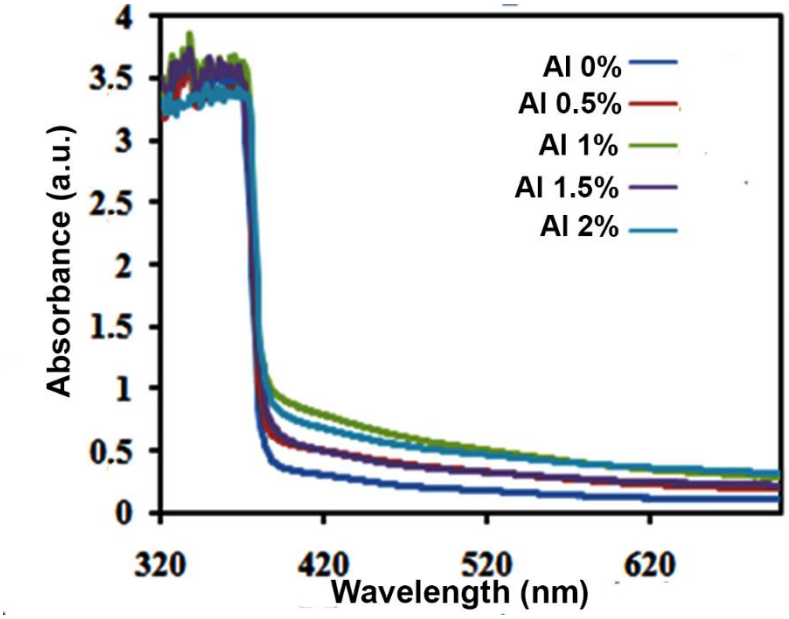

Figure 5. Spectra of UV-Vis absorption of the obtained ZnO nanorods.

Table 3 Direct band gap estimation of the samples

No	Al concentration (%)	Bnad gap (eV)
1	0.0	3.267
2	0.5	3.272
3	1.0	3.277
4	1.5	3.267
5	2.0	3.268
6	2.5	3.271

Bandgap energy is the distance between the conduction band and the valence band. Bandgap energy can be measured easily by extrapolating the curve plot $(\alpha hv)^2$ to (hv) [18]. The direct bandgap of all the samples is summarized in Table 3, and we can observe that the magnitudes are slightly different (~3.27 eV). The bandgap values obtained in our study are slightly lower than a previous study, which reported a bandgap value of 3.37 eV [3,4]. The decrease in the energy gap is due to the formation of an irregular (broken) lattice arrangement, resulting from the presence of doping atoms so as to produce several levels of energy under the conduction band [19]. Bandgap value can give an effect to the maximum power produced by the active material, which also directly influences the power conversion of the cells [20].

3.4 Cell Performances

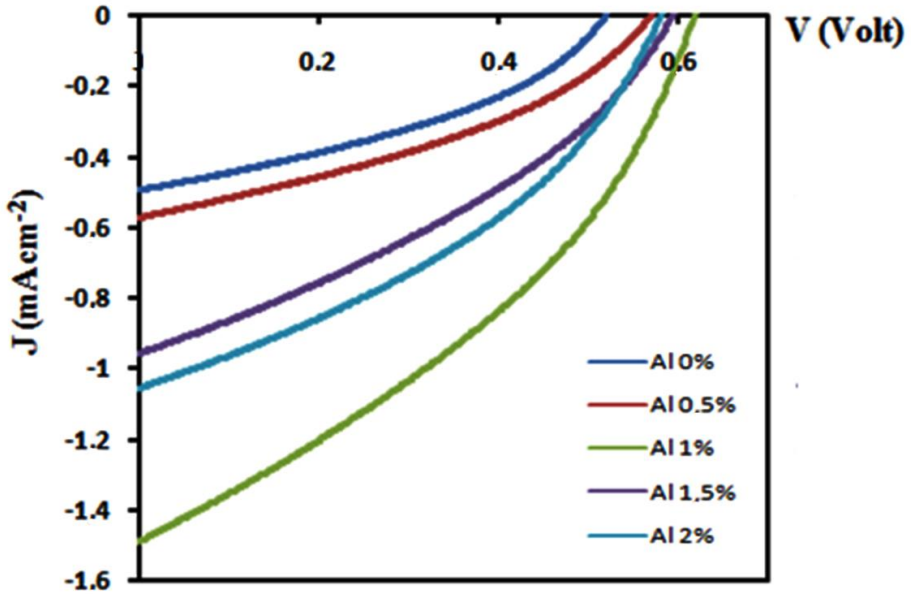

Figure 6 Plot of J-V of the fabricated DSSC under AM 1.5 G illumination.

Table 4. Photovoltaic performance of the fabricated DSSC

Concentration (%)	V_{OC} (V)	J_{SC} (mAcm^{-2})	V_{MPP} (V)	J_{MPP} (mAcm^{-2})	FF (%)	σ (Ω^{-1}m^{-1})	η (%)
0.0	0.518	0.493	0.339	0.291	0.383	0.029	0.098
0.5	0.569	0.573	0.395	0.339	0.591	0.031	0.122
1.0	0.617	1.490	0.381	0.879	0.590	0.057	0.335
1.5	0.593	0.863	0.351	0.563	0.348	0.035	0.198
2.0	0.581	1.060	0.365	0.635	0.601	0.046	0.232

Figure 6 is a J-V plot of the fabricated DSSC under 100 mW.cm^{-2} illumination. When cells are illuminated by light, increasing number of electrons are attracted to the conduction band, both from the active material and electrons originating from the dye [20]. The increase in the value of the current density at the maximum power point indicates that the number of electrons that flow through time is increasing [20-21]. As can be seen in Table 4, the optimum sample obtained in this study is 1.0% Al-doped ZnO nanorods, demonstrating an efficiency of 0.335%. The difference in the efficiency value between cells with and without Al doping is due to increased current density produced as a result of the input voltage [21]. The provision of Al doping at ZnO has a positive effect on DSSC efficiency, which can increase the efficiency up to 241.8%. This is because the administration of doping functions as an electric dopant so as to increase electrical conductivity [14]. The increase in efficiency is possibly due to the increase in magnitude of the current carrier Jsc and the conductivity σ by >2 orders, especially in the 1.0% Al sample.

4. CONCLUSION

Aluminum-doped ZnO nanorods with various doping concentrations of 0%, 0.5%, 1%, 1.5%, and 2% were successfully developed on FTO using a hydrothermal method with growth temperature of 90° C for 8 h. The diameter and thickness of the ZnO nanorods ranged from 122.8 to 602.9 nm and from 1.493 to 2.021 µm, respectively. The diffraction peaks of each sample at 2θ were 31.71°, 34.51°, 36.28°, 47.61°, and 56.54°, corresponding to a crystal plane of (100), (002), (101), (012), and (110), respectively. FWHM with a large percentage of variation of 0% to 2% of 0.2538 nm, 0.2431 nm, 0.2175 nm, 0.2319 nm and 0.2200 nm, respectively. The UV-Vis spectrum demonstrated that the absorption occurred between 320 and 385 nm. By 1% Al-doped concentration, the largest surface area and highest, with large crystal size and high absorption, could be achieved. The efficiencies of each dopant concentration were 0.098%, 0.122%, 0.335%, 0.198%, and 0.232%, respectively. The improvement effects of Al-doping to ZnO DSSC assist in enhancing the cell's efficiency to 214.83% than pristine ZnO.

ACKNOWLEDGEMENTS

The authors express fruitful thanks to DRPM Ministry of Research and Higher Education of Republic Indonesia through LPPM Universitas Riau for financial support this research in scheme of PDUPT (No. 764/UN.19.5.1.3/PT.01.03/ 2019) and HIKOM (No. 734/UN.19.5.1.3/PT.01.03/2019).

REFERENCES

[1] Grätzel, M. J. Photochem. Photobiol., A vol **164** issue 1-3 . (2004) pp. 3-14.

[2] Yella, A., Lee, H.-W., Tsao, H. N., Yi, C., Chandiran, A. K., Nazeeruddin, Md. K., Diau, E. W. -G., Yeh, C. -Y., Zakeeruddin, S. M., Gratzel, M. Science vol **334** issue 6056 (2011) pp. 629-634.

[3] Norton, D. P. Mat. Sci. Eng. R. vol. **43** (2004) pp. 139–247.

[4] Jie, J., Wang, G., Wang, Q., Chen, Y., Han, X., Wang, X., Hou, J.G. J. Phys. Chem. B. vol. **108** (2004) pp. 11976-11980.

[5] Iwantono I., Nurwidya W., Lestari L. R., Naumar F. Y., Nafisah S., Umar A. A., Rahman M. Y. A., Salleh M. M. J. Solid State Electrochem. vol **19,** issue 4 (2015) pp. 1217–1221.

[6] Lin, S.-S. Huang, J.-L., Saigalik, P. Surf. Coat. Technol., vol. **185**, issue 2–3, (2004) pp. 254–263.

[7] Soaram, K., Kim, S., Nam, G., Park, H., Yoon, H., Lee, S.-H., Kim, J. S., Kim, J. S., Kim, D. Y., Kim, S.-O., Leem, J.-Y. Bull. Korean Chem. Soc. vol. **34**, issue 4(2013) pp. 1205-1211.

[8] Maldonado F., Stashans, A. J. Phys. Chem. Solids, vol. **71**, issue 5, (2010) pp. 784-787.

[9] Nunes, P., Fortunato, E., Tonello, P., Fernandes, F. B., Vilarinho, P., Martins, R. Vacuum, vol. **64** (2002) no. 3-4, pp. 281-285.

[10] Vadivel, M., Babu, R.R., Arivanandhan, M., Ramamurthi, K., Hayakawa, Y. RSC Adv. **5** (2015) 27060-27068.

[11] Bindhu, M.R., Umadevi, M., Micheal, M.K., Arasu, M.V., Al-Dhabic, N.A. Mater. Lett. vol. **166** (2016) 19-22.

[12] Ridha, N. J., Jumali, M. H. H., Akrajas, A. A., Alosfur, F. Int. J. Electrochem. Sci., vol. **8** (2013) pp. 4583-4593.

[13] Zhou, H. M., Yi, D. Q., Yu, Z. M., Xiao, L. R., Li, J. Thin Solid Films, vol. **515**, issue 17 (2007) pp. 6909–6914.

[14] Alkahlout, A., Al-Dahdoudi, N., Grobelsek, I., Jilavi, M., De-Oliveira, P. W. J. Mater., vol. **2014** (2014) Article ID 235638, 8 pages.

[15] Lee, S.-H. , Han, S.-H., Jung, H. S., Shin, H., Lee, J., Noh, J.-H., Lee, S., Cho, I.-S., Lee, J.-K., Kim, J., Shin, H. J. Phys. Chem. C, vol. **114** (2014) issue 15, pp. 7185–7189.

[16] Suryanarayana, C., Norton, C. Grant, M. "X-ray diffraction a practical approach," New York, NY, USA: Springer US, (1998).

[17] Chanda, A., Geeta R. Mutta, G. R., Gupta, S., Singh, J. RSC Adv. vol **7** (2017) pp. 50527–50536.

[18] Irannejad, I., Janghorban, K., Tan, O. K., Huang, H., Lim, C. K., Tan, P. Y. Fang, X., Chua, C. S., Maleksaeedi, S., Hejazi, S. M. H., Shahjamali, M. M., Ghaffari, M. Electrochim. Acta, vol. **58** (2017) pp. 19-24.

[19] Prajapati, S., Kushwana, A., Sahay, P. P. J. Mater. Chem. Phys., vol. **142** (2013) issue 1 pp. 276-285.

[20] Lupan, O., Shishiyanu, S., Uraski, U., Khallaf, H., Chow, L., Shishiyanu, T., Sontea, V., Monaico, E., Railean, S. Sol. Energy Mater. Sol. Cells, vol. **93**, issue 8 (2009) pp. 1417–1422.

[21] Ko, H. Y., Kim, M. S., Yu, J. S., Appl. Surf. Sci., vol. **259** (2012) pp. 99-104.